# Comparative Analysis and Validation of Different Modulation Strategies for an Isolated DC-DC Dual Active Bridge Converter

Sergio Coelho(✉), Tiago J. C. Sousa, Vitor Monteiro, Luis Machado, Joao L. Afonso, and Carlos Couto

Centro ALGORITMI, University of Minho, Campus de Azurém, Guimarães, Portugal
sergio.coelho@algoritmi.uminho.pt

**Abstract.** This paper presents a comparative analysis of different modulation techniques that can be applied to a dual active bridge (DAB) converter, validating and analyzing its performance with the realization of computational simulations.

A DAB converter is an isolated dc-dc topology with great applicability in the most diverse branches of power electronics, as is the case of energy storage systems, solid state transformers, power electronic traction transformers, and, more recently, dc or hybrid microgrids. In this sense, several strategies have been studied to mitigate circulating currents, expand the zero voltage switching operating range, and reduce reactive power, as well as semiconductor stress. One of the possible solutions to increase the efficiency of this dc-dc converter is to adopt specific modulation techniques, however, it is necessary to assess which one has a better cost-benefit ratio. Thus, this paper presents a comparative analysis between: (i) Duty-cycle modulation; (ii) Single phase shift (SPS); (iii) Dual phase shift (DPS); (iv) Extended phase shift (EPS); (v) Triple phase shift (TPS). Specifically, this comparative analysis aims to investigate the performance of a DAB converter when controlled by the aforementioned strategies and operating with a nominal power of 3.6 kW, a switching frequency of 100 kHz, and a transformation ratio of 2:1. Considering these operation parameters and by analyzing the obtained simulation results, it was shown that only SPS, DPS, and TPS modulation techniques are considered suitable for this particular case. Duty-cycle modulation presents time limitations during the power transfer, whilst EPS is more suitable for dynamic medium/high power applications since it is capable of transferring a certain power value in a short period of time.

**Keywords:** Dual active bridge converter · Duty-cycle modulation · Single phase shift · Dual phase shift · Extended phase shift · Triple phase shift

## 1 Introduction

The dual active bridge (DAB) converter was firstly introduced in [1] for the purpose of practical implementation in medium/high power applications, as is the case of aerospace


J. L. Afonso et al. (Eds.): SESC 2020, LNICST 375, pp. 30–49, 2021.
https://doi.org/10.1007/978-3-030-73585-2_3

systems. Since this converter is capable of providing galvanic isolation and operate in a high-frequency regime, its power density is necessarily higher and, consequently, its passive components are considered to have less volume and weight [2]. In this sense, according to the latest trends and technologic advances in the field of power electronics (digital signal processors, semiconductors based on GaN and SiC, etc.), the study and applicability of the DAB converter have been receiving special prominence in the interface with energy storage systems, in the design of on board battery chargers for electric vehicles (EV) [3], in the mitigation of power quality problems [4], in solid state transformers [5], in power electronic traction transformers [6] and, more recently, in medium/low voltage dc (or hybrid) power grids, such as smart microgrids [7, 8].

Given that the architecture of a DAB converter is considered quite simple and symmetric, in which two H-bridges are connected by a high-frequency transformer (Fig. 1), a great number of advantages are provided to this topology when compared to the remaining high-frequency dc-dc converters referred in the literature. The latter include the dual active half bridge and the full bridge forward topologies, covered in [9] and [10], respectively. Besides the bidirectional operation and the galvanic isolation, common to the three topologies, the soft-switching capacity is also considered through the entire power range, and there is the possibility of including more degrees of freedom in the control algorithms.

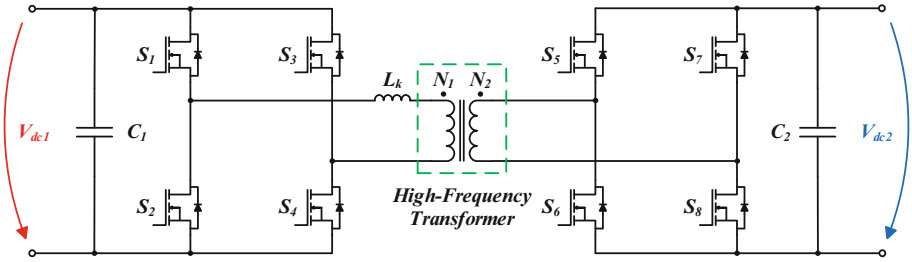


**Fig. 1.** Dual active bridge (DAB) converter.

However, to further increase the efficiency of this isolated dc-dc converter, new topologies derived from DAB have recently emerged, as is the case of the three-level DAB converter with five control degrees of freedom [11], the neutral point clamped DAB converter [12], the multilevel dc-dc DAB converter utilizing an *LCL* filter at the transformer side [13] and the dual bridge series resonant converter [14], which, compared to the traditional DAB, has as main features two resonant tanks and a tapped-transformer in order to increase the soft-switching range of the converter. In turn, in [15] the feasibility of connecting two DAB converters in parallel is studied, so that the efficiency of the system is optimized for different voltage and power demand levels.

Consequently, verifying the applicability of the DAB converter in low power systems, where the total losses must necessarily be as low as possible, new modulation techniques have been developed in order to regulate the current and voltage values of the system [16, 17]. Additionally, it is vital that a DAB converter assumes a dynamic behavior in the face of transient states and oscillations in the operating conditions. Therefore, in [18] a dynamic algorithm is implemented, capable of controlling each semiconductor independently, modifying their duty-cycle value in transient states. Such a measure would allow to eliminate current offsets (both the current that flows through the leakage inductance ($i_{L_k}$) and the magnetization current of the transformer) and, consequently, mitigate peak currents in the semiconductors. Similarly, in [19] the implementation of a linear quadratic regulator control based on linear matrix inequalities is considered to provide higher efficiency to the DAB converter when there is great uncertainty in the operating parameters of the system.

Increasing the efficiency of the DAB converter mainly involves the adoption of the latest generation semiconductors (SiC, GaN, etc.) and the reduction of the reactive power [20] and circulating current [21] values. However, in [22] issues related to possible transformer saturation and current peaks in systems that require a fast dynamic response are addressed, while in [23], is verified the attenuation of current stress in each of the semiconductors that make up the DAB converter architecture. In [24], a modulation strategy with 4 degrees of freedom is implemented with the goal of minimizing the total system losses. To this end, the necessary conditions to achieve soft-switching throughout the entire range of the DAB converter were considered and minimum-tank-current strategies were adopted in order to reduce the reactive power to zero value. To achieve the same objective, i.e., maximize the efficiency of the DAB converter, in [25] and in [26], a voltage offset is introduced to the dc blocking capacitors present on each side of the DAB, reducing, consequently, $i_{L_k}$.

Nonetheless, to regulate the power flow to and from each side of the DAB converter, the (traditional) single phase shift (SPS) modulation is often used. Such common use of this type of modulation is mainly due to its ease of implementation, however, high values of reactive power and circulating current are generated, thus making it difficult to implement zero voltage switching (ZVS) techniques. The expansion of the ZVS operating range is particularly relevant throughout the design and development of a DAB converter, which is why, in the literature, different methods and conditionings are studied to achieve this same objective. In [27] is presented a control technique capable of overcoming energy efficiency problems (among them the ZVS range limitations) that would arise in situations where the input voltage ($v_{dc1}$) does not match $n \bullet v_{dc2}$, with $v_{dc2}$ being the DAB output voltage and $n$ the transformation ratio of the high-frequency transformer. On the other hand, in [28] is verified the impact of dividing the leakage inductance ($L_k$) in the ZVS operating range. In turn, to expand this range, in [29], a control strategy for high-voltage applications is presented, in [30] a modulation for applications with wide input/output voltage is addressed and, lastly, in [31] the employability of a dual-transformer-based DAB converter is considered.

Among all the aforementioned methods, the ZVS operating range can also be expanded with the implementation of one of three phase shift modulation techniques: dual phase shift (DPS), extended phase shift (EPS) [32], and triple phase shift (TPS) [33]. These are based on the addition of more degrees of freedom to the system and seen as essential to mitigate energy efficiency problems, as is the case of semiconductor high-current stress [34]. Among the four main variants of the phase shift modulation (SPS, DPS, EPS, and TPS), the primary difference lies in the value assigned to each of the phase-lag angles, either between the two H-bridges (outer phase angle, $D_0$) or between the legs of each of the bridges (inner phase angles, $D_1$ and $D_2$, applied depending on the chosen modulation technique). The adoption of each one of these techniques, as mentioned above, will have a direct consequence on the efficiency presented by the DAB converter, however, the implementation difficulty will also be different. Normally, the value of $D_0$ controls the direction and the value of the transferred power to and from each side of the DAB converter, while $D_1$ and $D_2$ regulate and expand the ZVS range and minimize the circulating current, reactive power, and current peaks.

However, to mitigate faults, efficiency and reactive power problems, and possible power fluctuations, new modulation techniques, derived from the four above, have emerged. In this sense, in [35] and in [36] are presented derivations of the TPS and EPS modulation, both aiming to suppress the occurrence of transient dc bias. In [37] and [38], an improved/cooperative TPS modulation is presented, capable of mitigating dual-side circulating currents. A new DPS variant is considered in [39]. In [40] a unified phase shift modulation is studied, commonly used in dynamic systems, as is the case of electric traction drive systems. The latter is responsible for reducing peak currents during the moments that, e.g., fluctuations in the input voltage value occur. In [41], a flux control modulation is exposed, derived from SPS, which aims to keep the utilization of the transformer core constant on the whole load range during power transfer. Lastly, in [42] a novel hybrid current modulation is presented, based on triangular current modulation and trapezoidal current modulation techniques, which aims to reduce THD problems without increasing the stress caused in semiconductors and the RMS value of the DAB current.

Despite already existing comparative studies on the application of the aforementioned phase shift modulation techniques (SPS, DPS, EPS, and TPS) [43–46], no reference compares the four techniques simultaneously, representing the main contribution of this paper. In addition, it would be important to verify the behavior of the DAB converter when operating as a single active bridge (SAB), i.e., when only one H-bridge is switching, with the other adopting a passive behavior (current flowing through diodes). In this sense, this paper organizes as follows: Sect. 1 introduces the main ideas adjacent to this paper, presenting, at the same time, a review on the state-of-the-art. The operating principle of the system is referred in Sect. 2, while Sect. 3 describes each modulation technique applied to the DAB converter, explaining their advantages and disadvantages. Additionally, the obtained simulation results (performed with PSIM 9.1) are also compared in this section, observing current and voltage waveforms in the high-frequency transformer and in the resistive load, as well as the triggering gate signals of each semiconductor. Lastly, the main conclusions of this scientific article are presented.

## 2 Operating Principle of the System

As aforementioned, the adoption of the correct modulation strategy for the DAB converter will be translated into a great number of advantages in terms of energy efficiency. Thereby, in the first instance, it is crucial to define the operating characteristics of the system, so that, subsequently, each modulation technique can be analyzed and discussed in greater detail. The parameters of the DAB converter and respective values are shown in Table 1, however, it is important to note that they will remain constant throughout the simulations of each type of modulation. This measure was adopted to approximate the performed simulations to a real application case, where the physical components cannot be changed depending on the chosen control technique.

Among all the values presented in Table 1, it is important to highlight the values assigned to the switching frequency ($f_{sw}$) and to the $L_k$. The choice of such a high value for $f_{sw}$ meets the recent trends in power electronics systems (SiC and GaN-based semiconductors) and enables the compaction of the system in case of possible implementation, allowing, consequently, the reduction in the volume and weight of inductors and capacitors. On the other hand, the value of $L_k$ was selected in order to obtain the best compromise between the expansion of the ZVS range and the total losses of the DAB. As (1) demonstrates, the latter are the result of the sum of conduction losses ($P_{cond}$), switching losses ($P_{sw}$), losses in the transformer ($P_{tr}$) and, lastly, losses in $L_k$ ($P_{L_k}$).

$$P_t = P_{cond} + P_{sw} + P_{tr} + P_{L_k} \tag{1}$$

**Table 1.** Operating characteristics of the DAB converter

| Parameter | Value | Unit |
|---|---|---|
| Primary side dc-link voltage, $v_{dc1}$ | 400 | V |
| Secondary side dc-link voltage, $v_{dc2}$ | 200 | V |
| Nominal operating power | 3600 | W |
| Switching frequency, $f_{sw}$ | 100 | kHz |
| Sampling frequency, $f_s$ | 50 | kHz |
| Transformation ratio, $n$ | 2:1 | – |
| Leakage inductance (primary), $L_k$ | 3.5 | μH |
| Primary side dc-link capacitor, $C_1$ | 1680 | μF |
| Secondary side dc-link capacitor, $C_2$ | 1680 | μF |
| Secondary side resistive load | 11.11 | Ω |

## 3 Simulation Results of Each Modulation Technique

As mentioned, each modulation technique will be studied and validated in this section through the implementation of computer simulations, comparing voltage and current waveforms in the most diverse points of the DAB converter. On the other hand, the triggering gate signals of the semiconductors $S_1$, $S_3$, $S_5$ e $S_7$ are shown, essential to the detailed study proposed in this paper.

### 3.1 DAB Operating as a Single Active Bridge (SAB) Converter Under Duty-Cycle Modulation

With the implementation of this modulation technique, it is intended to demonstrate the behavior of the system presuming the choice of a SAB topology, in which one of the H-bridges enables switching under the duty-cycle modulation, whilst the other assumes a passive behavior since it will be the semiconductor's free-wheeling diodes who provides a path for the current. Such architecture facilitates the implementation of this modulation technique and provides greater robustness to the system. Thus, in order to regulate the voltage on the secondary dc-link ($v_{dc2}$) at 200 V (previously established reference value), a PI control algorithm was used, acting directly on the duty-cycle of the semiconductors $S_1$ and $S_3$, as can be seen in Fig. 2.

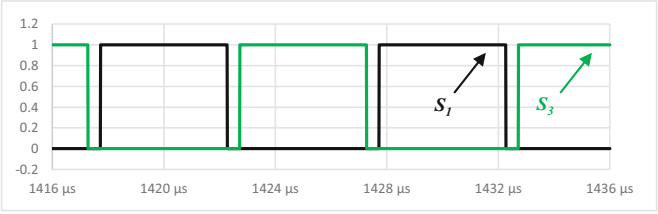


**Fig. 2.** Triggering gate signals of the semiconductors $S_1$ and $S_3$ using duty-cycle modulation.

Therefore, the current and voltage waveforms in the high-frequency transformer were monitored during a moment that $v_{dc2}$ is very close to its steady-state reference value (200 V). As shown in Fig. 3 (a), the currents in the primary and secondary side of the transformer ($i_{pri}$ and $i_{sec}$), despite having, respectively, peaks of 17.51 A and 35.02 A, present a null mean value and are in phase with the voltage waveforms at the terminals of the transformer ($v_{pri}$ and $v_{sec}$). Moreover, it is verified that $i_{pri}$ always takes half the instantaneous value of $i_{sec}$, thus respecting the applied transformation ratio. On the other hand, $v_{pri}$ and $v_{sec}$ can be observed in Fig. 3 (b), and, through their analysis, it is verified that $v_{sec}$ has a maximum value close to 200 V, thus proving the veracity of the applied control algorithm.

Since $v_{sec}$ is representative of the reflection of $v_{pri}$ on the secondary side, the transfer of energy in the high-frequency transformer is slower and more limited, a direct consequence of the gradual, and also slower, increase of $i_{pri}$. In this way, it is possible to conclude that the energy transfer range is quite short and time consuming. Through the

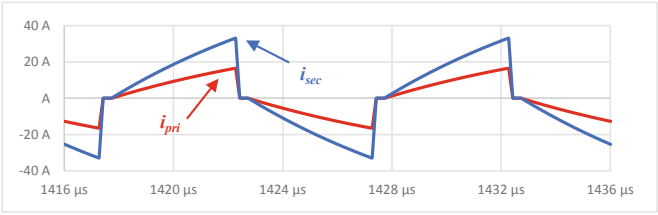


(a)

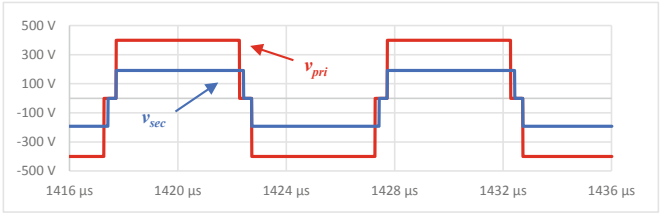


(b)

**Fig. 3.** Waveforms in the primary and secondary side of the high-frequency transformer using duty-cycle modulation: (a) Currents; (b) Voltages.

analysis of Fig. 3 (b), it is possible to verify a small mismatch between $v_{pri}$ and $v_{sec}$, caused by the voltage drop in $L_k$. The lower the value of $L_k$, the lower the voltage drop, the aforementioned mismatch, and the current peaks in the high-frequency transformer.

Finally, as shown in Fig. 4, the load current ($i_{load\_sec}$) has a mean value of 17.255 A, reason why the operating power of the system is slightly below the desired 3.6 kW.

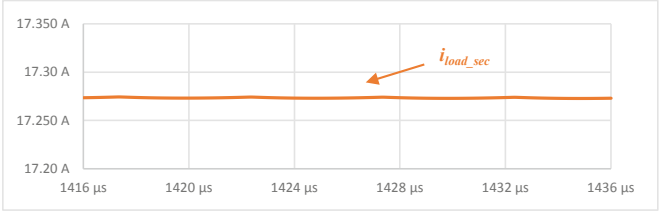


**Fig. 4.** Load current using duty-cycle modulation

### 3.2 Single Phase Shift (SPS)

The phase shift modulation techniques, compared to the aforementioned duty-cycle modulation, present a large number of advantages, highlighting the efficiency provided to the isolated dc-dc converters and the fact that all semiconductor gate signals have a fixed duty-cycle of 50%. Regardless of the direction of the power, each of the eight semiconductors is always switching and, as mentioned, with a constant duty-cycle. However, the phenomenon that allows the power transfer to and from each side of the DAB converter

is the mismatch between the voltages at the terminals of the high-frequency transformer. These two signals, when phase shifted, generate a voltage in $L_k$ and, consequently, a certain current will flow through it ($i_{L_k}$). Depending on whether the phase shift is positive or negative, the direction of $i_{L_k}$ will be changed and the power will flow in accordance. In other words, if $v_{pri}$ is ahead of $v_{sec}$, the power will flow from the primary side to the secondary one. If the opposite happens, power will flow from the secondary to the primary. It will be the adjustment of the phase mismatch between $v_{pri}$ and $v_{sec}$ that will regulate the value of transferred power: the higher its value, the greater the transferred power. However, as aforementioned, for simplicity reasons, this paper only analyzes the power flow from the primary to the secondary side.

In systems in which the value of $v_{dc1}$ is very close to $v_{dc2}$, SPS modulation is usually used. However, the great limitation of this technique is the existence of only one degree of freedom, i.e., the only variable that can be controlled is the phase angle between each of the H-bridges (outer phase angle, $D_0$). This fact leads to higher reactive power values and circulating currents in the DAB, especially in times of non-correspondence in the voltage values on each side ($v_{dc1} \neq nv_{dc2}$). Thus, the converter losses tend to be naturally higher, as well as the current peaks in the semiconductors.

For this particular application case, the value of $D_0$ will be generated using a PI algorithm, resulting from the comparison between the reference of 200 V and the measured value of $v_{dc2}$. Since only degree of freedom is considered, the waveform of $v_{pri}$ and $v_{sec}$ presents two voltage levels, as can be seen in Fig. 5 (a). Looking at this figure, it is possible to verify that $v_{sec}$ is delayed in relation to $v_{pri}$, thus proving the energy transfer from the primary side to the secondary one. This phase shift represents the value generated by the PI algorithm and can be seen in greater detail in Fig. 5 (b).

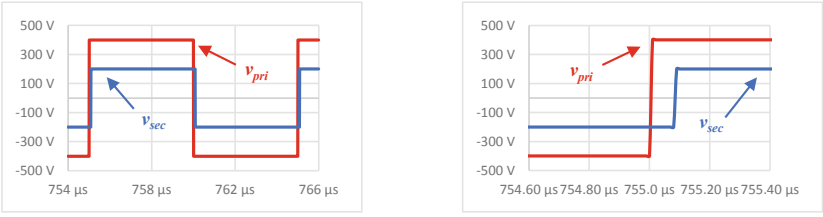


**Fig. 5.** Voltage waveforms in the primary and secondary side of the high-frequency transformer using SPS modulation: (a) During a complete cycle; (b) In detail.

In Fig. 6, on the other hand, the current waveforms on each side of the high-frequency transformer are shown. As in the duty-cycle modulation technique (operating as SAB), these have null mean value and are in accordance with the $v_{pri}$ and $v_{sec}$ waveforms, i.e., the currents have a positive value when the voltage is also positive, the same happening for the situation when the current is negative.

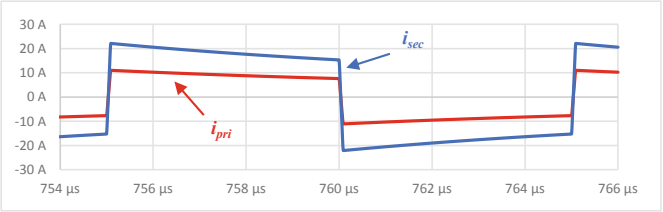


**Fig. 6.** Current waveforms in the primary and secondary side of the high-frequency transformer using SPS modulation.

Figure 7 shows the voltage and current waveforms in the resistive load connected in parallel with the secondary dc-link. As it can be seen, in steady-state, the voltage assumes an average value of 199.03 V while the current is at 17.915 A. Thus, the active power in the load has an approximate value of 3.566 kW, a value considered very close to the desired one (3.6 kW).

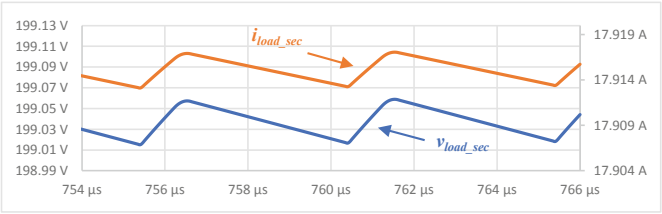


**Fig. 7.** Voltage and current waveforms in the resistive load in steady-state using SPS modulation.

In turn, Fig. 8 shows the triggering gate signals of each leg upper semiconductor ($S_1$, $S_3$, $S_5$, and $S_7$). As mentioned, the SPS technique only considers one degree of freedom, the reason why in Fig. 8 (a) the gate signals of the semiconductors $S_1$ and $S_3$ are 180° phase shifted. This same degree of freedom is related to the existing phase shift between the two H-bridges ($D_0$), visible in Fig. 8 (b), where $S_5$ assumes a delay of 2.88° in relation to $S_1$. Lastly, since the gate signal applied to $S_7$ is 180° phase shifted from the one applied to $S_5$, in Fig. 8 (c) the sum of this 180° mismatch with the value of $D_0$ is shown, thus making a total phase lag of 182.88° between $S_1$ and $S_7$. It should also be noted that, as expected, the PWM signals applied to $S_2$, $S_4$, $S_6$, and $S_8$ will be complementary to the ones showed in Fig. 8.

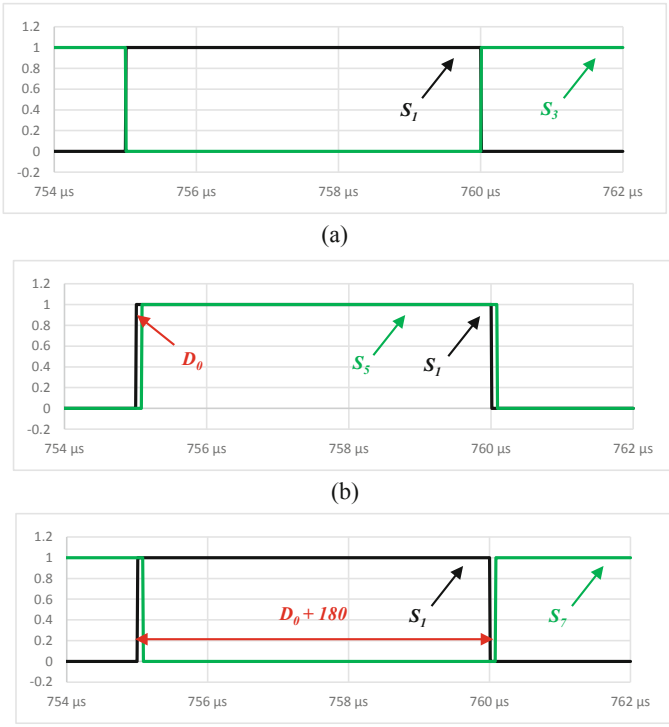


**Fig. 8.** Triggering gate signals using SPS modulation: (a) $S_1$, $S_3$; (b) $S_1$, $S_5$; (c) $S_1$, $S_7$.

### 3.3 Dual Phase Shift (DPS)

The DPS modulation, compared to SPS, contemplates a new degree of freedom, thus making a total of two. These degrees of freedom are related to the phase shift between the two H-bridges ($D_0$, as for the SPS) and the legs of each H-bridge (inner phase angle, $D_1$). With the addition of $D_1$, the efficiency of the DAB is improved, since the value of reactive power, circulating currents, and current peaks will be reduced. Although the ZVS operating range is not considered in these simulations, in theory, it could also be expanded. On the other hand, the inclusion of $D_1$ will also allow obtaining a three level voltage waveform at the terminals of the high-frequency transformer, but to really optimize energy efficiency levels, the values of $D_0$ and $D_1$ must be calculated based on duty cycle and phase shift modulations. Thus, as in the SPS technique, the value of $D_0$ will be obtained using a PI algorithm, whereas, $D_1$ will be calculated with the aid of (2) and (3). This equation will vary the value of $D_1$ according to the relation between $v_{dc1}$ and $v_{dc2}$, being as much greater as the value of the ratio.

The values of $D_0$ and $D_1$ can be observed in Fig. 9 (a) and Fig. 9 (b), respectively. In the image presented below, the triggering gate signals of $S_1$, $S_3$, $S_5$, and $S_7$ using DPS modulation are shown. By analyzing Fig. 9, it is observed that the signals applied to $S_3$,

$S_5$, and $S_7$ are ahead of $S_1$, thus proving the energy flow direction. In turn, Fig. 9 (c) a comparison is made between the signals applied to $S_1$ and $S_7$, lagged $D_0 + D_1$ degrees.

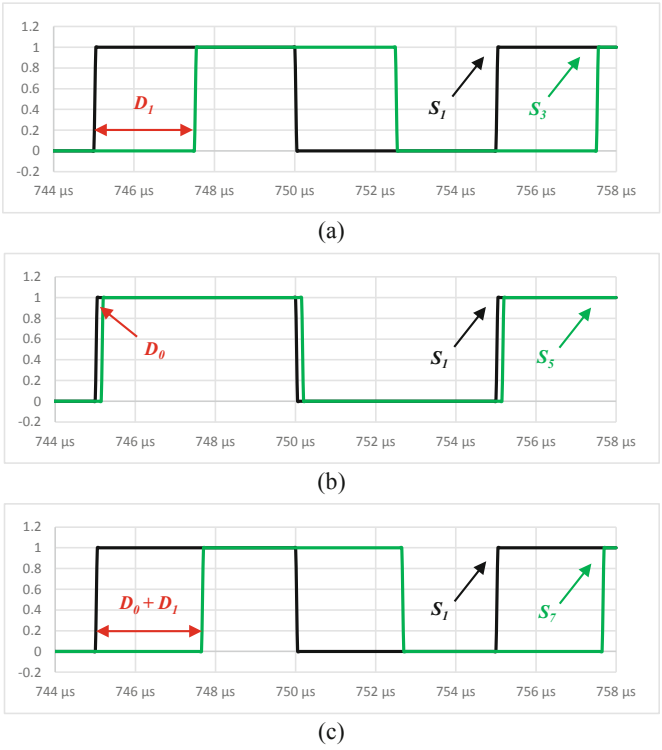


**Fig. 9.** Triggering gate signals using DPS modulation: (a) $S_1$, $S_3$; (b) $S_1$, $S_5$; (c) $S_1$, $S_7$.

$$error = \left| n - \frac{v_{dc1}}{v_{dc2}} \right| \tag{2}$$

$$D_1 = 180\, e^{-2.197\, error} \tag{3}$$

As mentioned, with the addition of a new degree of freedom, a voltage waveform with three levels will be generated at the terminals of the high-frequency transformer. Given the higher number of levels, the efficiency of this magnetic element will also be higher and the THD significantly lower, which is why multilevel topologies have received special prominence in power electronics systems to mitigate power quality problems. The waveforms of $v_{pri}$ and $v_{sec}$ are presented in Fig. 10, being possible to clearly observe the existing phase lag between them. Thus, with $v_{pri}$ ahead of $v_{sec}$, it is proven, once again, the direction of the energy flow.


**Fig. 10.** Voltage waveforms in the primary and secondary side of the high-frequency transformer using DPS modulation.

In addition, in Fig. 11 are shown the current waveforms in the high-frequency transformer with the employment of a DPS modulation. By analyzing this graphic, it is concluded that, once again, the mean value of these currents is null, even if the latter does not assume zero value when $v_{pri}$ and $v_{sec}$ does. Although the current peak is higher than in SPS modulation, the stress will be much lower.

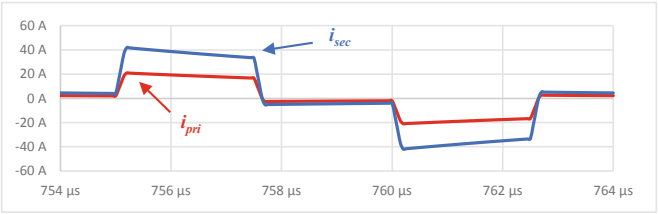


**Fig. 11.** Current waveforms it the primary and secondary side of the high-frequency transformer using DPS modulation.

However, it is also necessary to monitor and regulate the voltage on the secondary dc-link, being essential to maintaining its level close to the 200 V reference. In Fig. 12 it is shown the regulation of $v_{dc2}$ at a transient state, in which $t = 0.63$ ms is representative of the moment that the switching signals of the secondary bridge are enabled. With the adoption of this measure, a pre-charge of the dc-link capacitors is carried out, thus avoiding overcurrent, reducing total losses, and guaranteeing the integrity of the hardware.

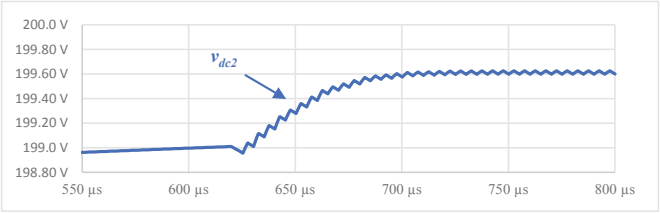


**Fig. 12.** Voltage waveform in the secondary dc-link during a transient state using DPS modulation.

### 3.4 Extended Phase Shift (EPS)

As mentioned in the introduction of this paper, the EPS modulation is normally employed in medium/high voltage power electronics systems. In this context, when compared to the SPS technique, EPS modulation is capable of reducing the values of circulating current and conduction losses when a large amount of power needs to be transferred to and from each side of an isolated dc-dc converter. Moreover, this technique enables and improves the soft-switching capacity of the converter and presents a large ZVS operating range.

However, in low power systems, as is the case, the EPS modulation has a reduced impact and may even provoke worse results than SPS. Under light load conditions, the operating range decreases, the reason why the obtained simulation results, compared to SPS modulation, show higher current peaks and semiconductor stress.

This modulation technique, as for DPS, considers two degrees of freedom, once again, related to the phase shift between $v_{pri}$ and $v_{sec}$ and between the legs of the primary H-bridge. In Fig. 13 (a), the influence $D_1$ is shown, being possible to observe the phase lag between $S_1$ and $S_3$. However, the difference between DPS and EPS lies in the signal applied to the semiconductor $S_7$: instead of adding the value of $D_0$ to $D_1$, during the EPS modulation, $S_7$ will be complementary to $S_5$, without considering the influence of $D_1$, as it is possible to observe in Fig. 13 (b) and in Fig. 13 (c).

As it can be seen in Fig. 14 (a), given the PWM signals applied to each semiconductor, voltages with different waveforms will be generated at the terminals of the high-frequency transformer, with $v_{pri}$ presenting three voltage levels ($v_{dc1}$, 0 and $-v_{dc1}$) and $v_{sec}$ only two ($v_{dc2}$ and $-v_{dc2}$).

Nonetheless, during the moments that $v_{pri}$ and $v_{sec}$ assume their respective absolute maximum values (400 V and 200 V, represented by $t_1$, $t_2$, and $t_3$ in the figures presented below), $i_{pri}$ and $i_{sec}$ increase more sharply, showing peak values that are not compatible with this application case (Fig. 14 (b)). A possible solution would be to increase the value of $D_1$ or decrease $D_0$, however, the regulation of $v_{dc2}$ to the reference value of 200 V would be impossible to achieve. In turn, in the event of a possible change in the DAB converter parameters, increasing the value of $L_k$ or the system's $f_s$, the current peaks of $i_{pri}$ and $i_{sec}$ would be considerably lower.

Lastly, and once again, the regulation of $v_{dc2}$ can be observed in Fig. 15 during a transient state, coincidental with the moment when the capacitor pre-charge is finished. As it is possible to contemplate, the steady-state value of $v_{dc2}$ is 202.7 V, thus resulting in a difference of 2.7 V for the pre-established reference.

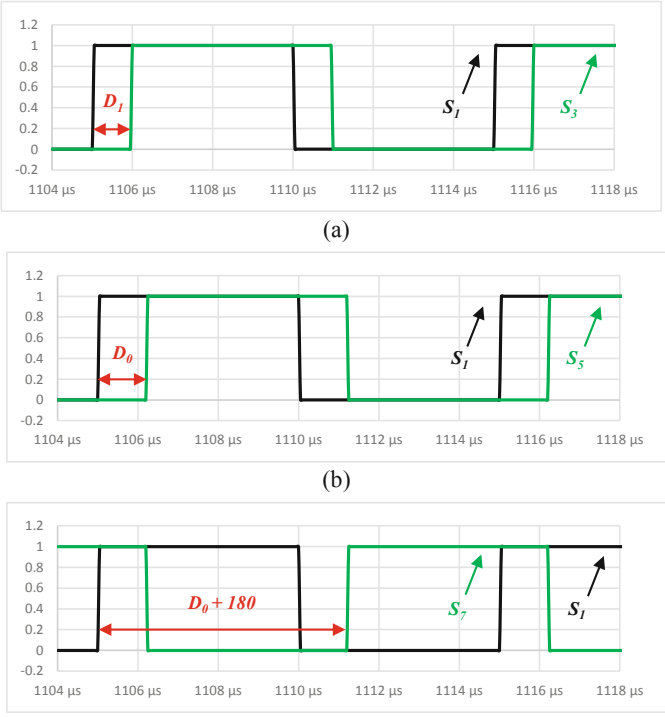


**Fig. 13.** Triggering gate signals using EPS modulation: (a) $S_1$, $S_3$; (b) $S_1$, $S_5$; (c) $S_1$, $S_7$.

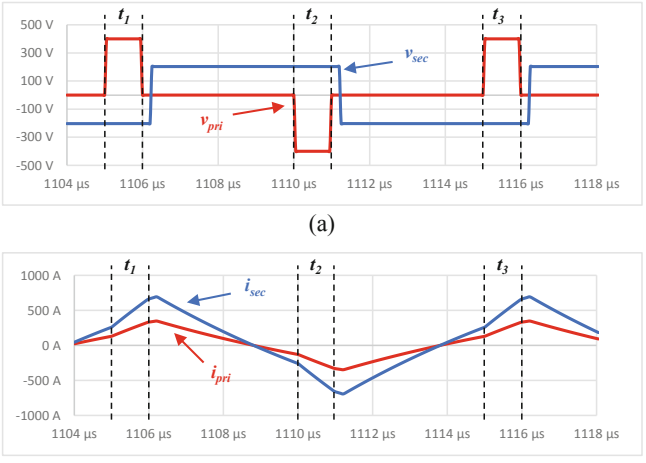


**Fig. 14.** Waveforms in the primary and secondary side of the high-frequency transformer using EPS modulation: (a) Voltages; (b) Currents.

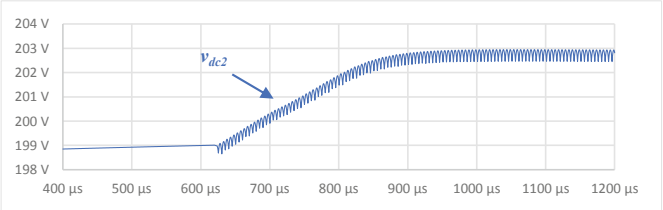


**Fig. 15.** Voltage waveform in the secondary dc-link during a transient state using EPS modulation.

### 3.5 Triple Phase Shift (TPS)

In this section, the obtained simulation results for the TPS modulation are analyzed. In the literature, among the five control techniques contemplated in this paper, TPS is considered the one with the best energy efficiency results, being capable of mitigating circulating currents and high reactive power values, change the RMS value of $i_{L_k}$, and, consequently, decrease the semiconductor stress. Such capability is obtained with the addition of a new degree of freedom to the system, making a total of three: the aforementioned $D_0$ and $D_1$ and a new inner phase angle ($D_2$), employed to the secondary H-bridge of the DAB converter. All the angles are independent of each other, which is why TPS modulation presents greater implementation difficulty. During the adoption of a SPS modulation, the signal applied to $S_7$ resulted from the sum of $D_0$ and $D_1$, a measure that is considered a limitation to the optimization of the soft-switching capacity and to the expansion of the ZVS range. In turn, during TPS modulation, the triggering gate signal applied to $S_7$ results from the sum of $D_0$ and $D_2$ (Fig. 16 (c)), i.e., the new degree of freedom here contemplated. The analysis of Fig. 16 (a) and Fig. 16 (b) shows that the triggering gate signals applied to $S_3$ and $S_5$ are similar to EPS and DPS cases, adding the value of $D_1$ and $D_0$, respectively, to the reference assigned to $S_1$.

Through the realization of computer simulations, it was concluded that the TPS technique, due to the inclusion of a new degree of freedom, is a very flexible modulation, capable of being applied in low power systems, which was not the case for EPS. As Fig. 17 (a) shows, with the adjustment of the value of $D_2$ it is possible to change the time that $v_{sec}$ assumes its absolute maximum value (200 V), allowing the energy transfer at a higher or reduced rate, depending on the application case. That fact can be confirmed by the analysis of Fig. 17 (b), in which $i_{pri}$ and $i_{sec}$ are presented.

It should also be noted that for the purpose of analyzing the behavior of the TPS modulation in the face of oscillations in the value of $D_2$, during the computational simulations the value of this angle was varied manually, i.e., without any control strategy applied. Nonetheless, when it is important to consider the expansion of the ZVS operating range, this value should be calculated based on appropriate strategies.

As was the case for the aforementioned modulation techniques, the regulation of $v_{dc2}$ is verified in Fig. 18, assuming a steady-state value of 199.8 V (extremely close to its reference, 200 V), thus proving the correct operation of the PI algorithm.

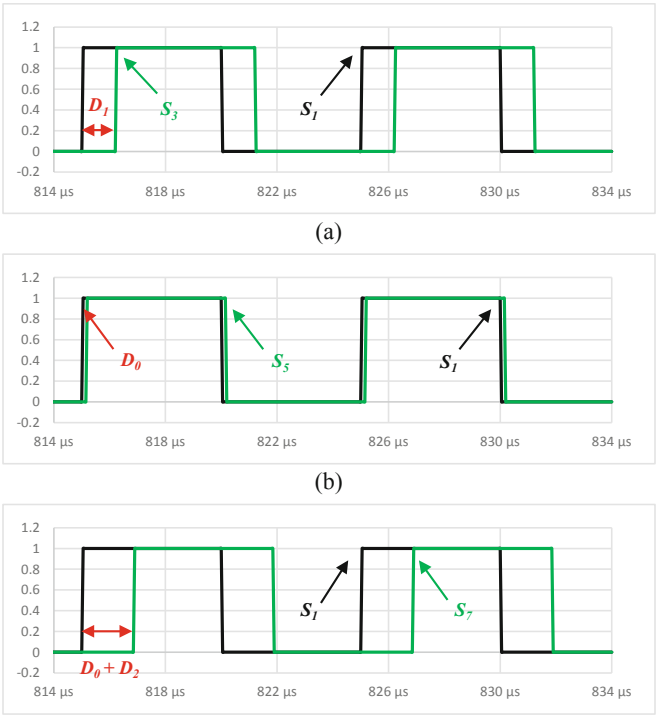


**Fig. 16.** Triggering gate signals using TPS modulation: (a) $S_1$, $S_3$; (b) $S_1$, $S_5$; (c) $S_1$, $S_7$.

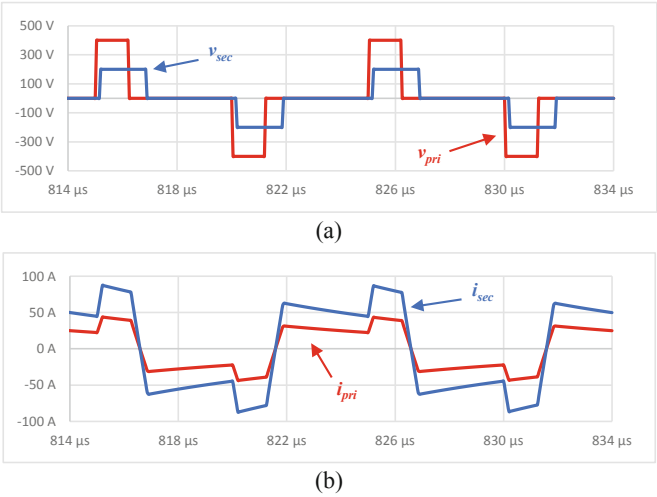


**Fig. 17.** Waveforms in the primary and secondary side of the high-frequency transformer using TPS modulation: (a) Voltages; (b) Currents.

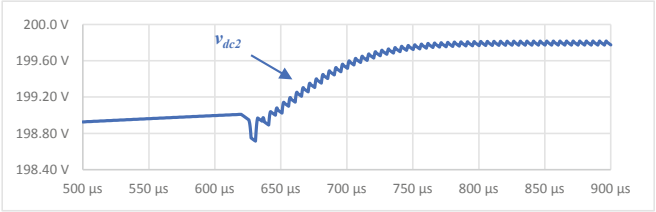


**Fig. 18.** Voltage waveform in the secondary dc-link during a transient state using TPS modulation.

## 4 Conclusions

Throughout the paper, five modulation techniques that could be applied to control a dual active bridge (DAB) converter were studied, namely duty-cycle modulation, single phase shift (SPS), dual phase shift (DPS), extended phase shift (EPS), and triple phase shift (TPS). The results obtained in computer simulations were later compared, showing the different triggering gate signals for each modulation and analyzing the current and voltage waveforms in the most diverse points of the DAB converter. In turn, these results were obtained for an operating power of 3.6 kW and a switching frequency of 100 kHz. Taking into account the assigned simulation parameters, it was possible to conclude that among all the aforementioned modulation techniques, only SPS, DPS, and TPS are suitable for this particular case. The duty-cycle modulation, when applied to a single active bridge (SAB) topology, presents great limitations during power transfer, since this process is carried out at a very low rate. On the other hand, the EPS modulation is more suitable for medium/high power electronics systems, being capable of transferring a certain power value in a short period of time, convenient for controlling high power dynamic systems with constant variations in its operating conditions. Lastly, among SPS, DPS and TPS modulation techniques, the last one is seen as the most flexible, since it enables three degrees of freedom (SPS presents one, and DPS two). However, its implementation difficulty is much higher and does not compensate the effort for this specific application case, being able to be applied in medium power systems that need to vary the RMS value of the current that flows through the leakage inductance.

**Acknowledgments.** This work has been supported by FCT – Fundação para a Ciência e Tecnologia within the Project Scope: UIDB/00319/2020. This work has been supported by the FCT Project PV4SUSTAINABILITY Reference: 333203230 and by the project newERA4GRIDs PTDC/EEI-EEE/30283/2017. Tiago Sousa is supported by the doctoral scholarship SFRH/BD/134353/2017 granted by FCT.

## References

1. de Doncker, R.W.A.A., Divan, D.M., Kheraluwala, M.H.: A three-phase soft-switched high-power-density DC/DC converter for high-power applications. IEEE Trans. Ind. Appl. **27**(1), 63–73 (1991). https://doi.org/10.1109/28.67533
2. Mueller, J.A., Kimball, J.W.: Modeling dual active bridge converters in DC distribution systems. IEEE Trans. Power Electron. **34**(6), 5867–5879 (2019). https://doi.org/10.1109/TPEL.2018.2867434

3. Dao, N.D., Lee, D.C., Phan, Q.D.: High-efficiency SiC-based isolated three-port DC/DC converters for hybrid charging stations. IEEE Trans. Power Electron. **35**(10), 10455–10465 (2020). https://doi.org/10.1109/TPEL.2020.2975124
4. Wang, D., Nahid-Mobarakeh, B., Emadi, A.: Second harmonic current reduction for a battery-driven grid interface with three-phase dual active bridge DC-DC converter. IEEE Trans. Industr. Electron. **66**(11), 9056–9064 (2019). https://doi.org/10.1109/TIE.2019.2899563
5. Sun, Y., Gao, Z., Fu, C., Wu, C., Chen, Z.: A hybrid modular DC solid-state transformer combining high efficiency and control flexibility. IEEE Trans. Power Electron. **35**(4), 3434–3449 (2020). https://doi.org/10.1109/TPEL.2019.2935029
6. Liu, J., Yang, J., Zhang, J., Nan, Z., Zheng, Q.: Voltage balance control based on dual active bridge DC/DC converters in a power electronic traction transformer. IEEE Trans. Power Electron. **33**(2), 1696–1714 (2018). https://doi.org/10.1109/TPEL.2017.2679489
7. Kwak, B., Kim, M., Kim, J.: Inrush current reduction technology of DAB converter for low-voltage battery systems and DC bus connections in DC microgrids. IET Power Electron. **13**(8), 1528–1536 (2020). https://doi.org/10.1049/iet-pel.2019.0506
8. Hu, J., Joebges, P., Pasupuleti, G.C., Averous, N.R., de Doncker, R.W.: A maximum-output-power-point-tracking-controlled dual-active bridge converter for photovoltaic energy integration into MVDC grids. IEEE Trans. Energy Convers. **34**(1), 170–180 (2019). https://doi.org/10.1109/TEC.2018.2874936
9. Chakraborty, S., Chattopadhyay, S.: Fully ZVS, minimum RMS current operation of the dual-active half-bridge converter using closed-loop three-degree-of-freedom control. IEEE Trans. Power Electron. **33**(12), 10188–10199 (2018). https://doi.org/10.1109/TPEL.2018.2811640
10. Roggia, L., Costa, P.F.S.: Comparative analysis between integrated full-bridge-forward and dual active bridge DC–DC converters. Electron. Lett. **54**(4), 231–233 (2018). https://doi.org/10.1049/el.2017.3326
11. Liu, P., Chen, C., Duan, S.: An optimized modulation strategy for the three-level DAB converter with five control degrees of freedom. IEEE Trans. Industr. Electron. **67**(1), 254–264 (2020). https://doi.org/10.1109/TIE.2019.2896209
12. Xuan, Y., Yang, X., Chen, W., Liu, T., Hao, X.: A novel NPC dual-active-bridge converter with blocking capacitor for energy storage system. IEEE Trans. Power Electron. **34**(11), 10635–10649 (2019). https://doi.org/10.1109/TPEL.2019.2898454
13. Chan, Y.P., Yaqoob, M., Wong, C.S., Loo, K.H.: Realization of high-efficiency dual-active-bridge converter with reconfigurable multilevel modulation scheme. IEEE J. Emerg. Sel. Top. Power Electron. **8**(2), 1178–1192 (2020). https://doi.org/10.1109/JESTPE.2019.2926070
14. Wu, J., Li, Y., Sun, X., Liu, F.: A new dual-bridge series resonant DC-DC converter with dual tank. IEEE Trans. Power Electron. **33**(5), 3884–3897 (2018). https://doi.org/10.1109/TPEL.2017.2723640
15. Rolak, M., Sobol, C., Malinowski, M., Stynski, S.: Efficiency optimization of two dual active bridge converters operating in parallel. IEEE Trans. Power Electron. **35**(6), 6523–6532 (2020). https://doi.org/10.1109/TPEL.2019.2951833
16. Jeung, Y.C., Lee, D.C.: Voltage and current regulations of bidirectional isolated dual-active-bridge DC-DC converters based on a double-integral sliding mode control. IEEE Trans. Power Electron. **34**(7), 6937–6946 (2019). https://doi.org/10.1109/TPEL.2018.2873834
17. Li, X., Wu, F., Yang, G., Liu, H., Meng, T.: Dual-period-decoupled space vector phase-shifted modulation for DAB-based three-phase single-stage AC-DC converter. IEEE Trans. Power Electron. **35**(6), 6447–6457 (2020). https://doi.org/10.1109/TPEL.2019.2950059
18. Takagi, K., Fujita, H.: Dynamic control and performance of a dual-active-bridge DC-DC converter. IEEE Trans. Power Electron. **33**(9), 7858–7866 (2018). https://doi.org/10.1109/TPEL.2017.2773267

19. Xia, P., Shi, H., Wen, H., Bu, Q., Hu, Y., Yang, Y.: Robust LMI-LQR control for dual-active-bridge DC-DC converters with high parameter uncertainties. IEEE Trans. Transp. Electrif. **6**(1), 131–145 (2020). https://doi.org/10.1109/TTE.2020.2975313
20. Shi, H., Wen, H., Chen, J., Hu, Y., Jiang, L., Chen, G.: Minimum-reactive-power scheme of dual-active-bridge DC-DC converter with three-level modulated phase-shift control. IEEE Trans. Ind. Appl. **53**(6), 5573–5586 (2017). https://doi.org/10.1109/TIA.2017.2729417
21. Karthikeyan, V., Gupta, R.: FRS-DAB converter for elimination of circulation power flow at input and output ends. IEEE Trans. Industr. Electron. **65**(3), 2135–2144 (2018). https://doi.org/10.1109/TIE.2017.2740853
22. Vazquez, N., Liserre, M.: Peak current control and feed-forward compensation of a DAB converter. IEEE Trans. Industr. Electron. **67**(10), 8381–8391 (2020). https://doi.org/10.1109/TIE.2019.2949523
23. Hebala, O.M., Aboushady, A.A., Ahmed, K.H., Abdelsalam, I.: Generic closed-loop controller for power regulation in dual active bridge DC-DC converter with current stress minimization. IEEE Trans. Industr. Electron. **66**(6), 4468–4478 (2019). https://doi.org/10.1109/TIE.2018.2860535
24. Yaqoob, M., Loo, K.H., Lai, Y.M.: A four-degrees-of-freedom modulation strategy for dual-active-bridge series-resonant converter designed for total loss minimization. IEEE Trans. Power Electron. **34**(2), 1065–1081 (2019). https://doi.org/10.1109/TPEL.2018.2865969
25. Liu, P., Duan, S.: A hybrid modulation strategy providing lower inductor current for the DAB converter with the aid of DC blocking capacitors. IEEE Trans. Power Electron. **35**(4), 4309–4320 (2020). https://doi.org/10.1109/TPEL.2019.2937161
26. Qin, Z., Shen, Y., Loh, P.C., Wang, H., Blaabjerg, F.: A dual active bridge converter with an extended high-efficiency range by DC blocking capacitor voltage control. IEEE Trans. Power Electron. **33**(7), 5949–5966 (2018). https://doi.org/10.1109/TPEL.2017.2746518
27. Xu, G., Sha, D., Xu, Y., Liao, X.: Hybrid-bridge-based DAB converter with voltage match control for wide voltage conversion gain application. IEEE Trans. Power Electron. **33**(2), 1378–1388 (2018). https://doi.org/10.1109/TPEL.2017.2678524
28. Xiao, Y., Zhang, Z., Andersen, M.A.E., Sun, K.: Impact on ZVS operation by splitting inductance to both sides of transformer for 1-MHz GaN based DAB converter. IEEE Trans. Power Electron. **35**(11), 11988–12002 (2020). https://doi.org/10.1109/TPEL.2020.2988638
29. Dung, N.A., Chiu, H.J., Lin, J.Y., Hsieh, Y.C., Liu, Y.C.: Efficiency optimisation of ZVS isolated bidirectional DAB converters. IET Power Electron. **11**(8), 1–8 (2018). https://doi.org/10.1049/iet-pel.2017.0723
30. Garcia-Bediaga, A., Villar, I., Rujas, A., Mir, L.: DAB modulation schema with extended ZVS region for applications with wide input/output voltage. IET Power Electron. **11**(13), 1–8 (2018). https://doi.org/10.1049/iet-pel.2018.5332
31. Xu, G., Sha, D., Xu, Y., Liao, X.: Dual-transformer-based DAB converter with wide ZVS range for wide voltage conversion gain application. IEEE Trans. Industr. Electron. **65**(4), 3306–3316 (2018). https://doi.org/10.1109/TIE.2017.2756601
32. Shi, H., et al.: Minimum-backflow-power scheme of DAB-based solid-state transformer with extended-phase-shift control. IEEE Trans. Ind. Appl. **54**(4), 3483–3496 (2018). https://doi.org/10.1109/TIA.2018.2819120
33. Shen, K., et al.: ZVS control strategy of dual active bridge DC/DC converter with triple-phase-shift modulation considering RMS current optimization. J. Eng. **2019**(18), 4708–4712 (2019). https://doi.org/10.1049/joe.2018.9341
34. Calderon, C., et al.: General analysis of switching modes in a dual active bridge with triple phase shift modulation. Energies **11**(9), 2419 (2018). https://doi.org/10.3390/en11092419
35. Bu, Q., Wen, H., Wen, J., Hu, Y., Du, Y.: Transient DC bias elimination of dual-active-bridge DC-DC converter with improved triple-phase-shift control. IEEE Trans. Industr. Electron. **67**(10), 8587–8598 (2020). https://doi.org/10.1109/TIE.2019.2947809

36. Dai, T., et al.: Research on transient DC bias analysis and suppression in EPS DAB DC-DC converter. IEEE Access **8**, 61421–61432 (2020). https://doi.org/10.1109/ACCESS.2020.2983090
37. Wu, F., Feng, F., Gooi, H.B.: Cooperative triple-phase-shift control for isolated DAB DC-DC converter to improve current characteristics. IEEE Trans. Industr. Electron. **66**(9), 7022–7031 (2019). https://doi.org/10.1109/TIE.2018.2877115
38. Luo, S., Wu, F., Wang, G.: Improved TPS control for DAB DC-DC converter to eliminate dual-side flow back currents. IET Power Electron. **13**(1), 32–39 (2020). https://doi.org/10.1049/iet-pel.2019.0562
39. Liu, X., et al.: Novel dual-phase-shift control with bidirectional inner phase shifts for a dual-active-bridge converter having low surge current and stable power control. IEEE Trans. Power Electron. **32**(5), 4095–4106 (2017). https://doi.org/10.1109/TPEL.2016.2593939
40. Hou, N., Song, W., Li, Y., Zhu, Y., Zhu, Y.: A comprehensive optimization control of dual-active-bridge DC-DC converters based on unified-phase-shift and power-balancing scheme. IEEE Trans. Power Electron. **34**(1), 826–839 (2018). https://doi.org/10.1109/TPEL.2018.2813995
41. Fritz, N., Rashed, M., Bozhko, S., Cuomo, F., Wheeler, P.: Flux control modulation for the dual active bridge DC/DC converter. J. Eng. **2019**(17), 4353–4358 (2019). https://doi.org/10.1049/joe.2018.8014
42. Zengin, S., Boztepe, M.: A novel current modulation method to eliminate low-frequency harmonics in single-stage dual active bridge AC-DC converter. IEEE Trans. Industr. Electron. **67**(2), 1048–1058 (2020). https://doi.org/10.1109/TIE.2019.2898597
43. Kumar, A., Bhat, A.H., Agarwal, P.: Comparative analysis of dual active bridge isolated DC to DC converter with single phase shift and extended phase shift control techniques. In: 2017 6th International Conference on Computer Applications in Electrical Engineering - Recent Advances, CERA 2017, vol. 2018-January, pp. 397–402 (2018). https://doi.org/10.1109/CERA.2017.8343363
44. Kumar, B.M., Kumar, A., Bhat, A.H., Agarwal, P.: Comparative study of dual active bridge isolated DC to DC converter with single phase shift and dual phase shift control techniques. In: 2017 Recent Developments in Control, Automation and Power Engineering, RDCAPE 2017, vol. 3, pp. 453–458 (2018). https://doi.org/10.1109/RDCAPE.2017.8358314
45. Kumar, A., Bhat, A.H., Agarwal, P.: Comparative analysis of dual active bridge isolated DC to DC converter with double phase shift and triple phase shift control techniques. In: 2017 Recent Developments in Control, Automation and Power Engineering, RDCAPE 2017, vol. 3, pp. 257–262 (2017). https://doi.org/10.1109/RDCAPE.2017.8358278
46. Kayaalp, I., Demirdelen, T., Koroglu, T., Cuma, M.U., Bayindir, K.C., Tumay, M.: Comparison of different phase-shift control methods at isolated bidirectional DC-DC converter. Int. J. Appl. Math. Electron. Comput. **4**(3), 68 (2016). https://doi.org/10.18100/ijamec.60506